Journal of Non-Newtonian Fluid Mechanics 344 (2025) 105454

Contents lists available at ScienceDirect

Journal of Non-Newtonian Fluid Mechanics

journal homepage: www.elsevier.com/locate/jnnfm

Full Length Article

Pair interactions of viscous drops suspended in a shear-thinning viscous and viscoelastic shear flow

Haoqian Wang , Anik Tarafder, Kausik Sarkar *

Department of Mechanical and Aerospace Engineering, The George Washington University, WA, DC 20052, USA

ARTICLE INFO

Keywords:
Pair-interaction
Viscoelasticity
Shear-thinning

ABSTRACT

Pair interactions of viscous (constant viscosity) drops suspended in a shear-thinning viscous and viscoelastic shear flow are numerically investigated using a front-tracking method. Apart from the usual passing trajectories, where drops interact and slide past each other in the streamwise direction, we note two new trajectories. Shear-thinning (power law index n <1) introduces reversed trajectories, where after interaction the drops reverse directions, and viscoelasticity (nonzero Weissenberg number Wi) gives rise to tumbling trajectories, where the drops revolve around each other. In a viscous medium, only passing and reversed trajectories are seen in an n-Ca phase plot. Passing trajectories transition into reversed ones for small n (more shear-thinning) and low capillary numbers Ca with the critical n for transition increasing with decreasing capillary number. In a viscoelastic medium, one finds all three trajectories in an n-Wi phase plot: reversed trajectories for low Wi and low n, tumbling for high Wi and high n, and passing trajectories in between. The trajectories are explained in terms of the streamline topology around a single drop in shear: a region of reversed streamlines due to shear-thinning, and a region of spiraling streamlines due to viscoelasticity, both effects being more prominent for low Ca values (less deformable drops). Physical reasoning for the reversed streamlines in the presence of shear-thinning is offered, relating it to the pressure field.

1. Introduction

The dynamics of rigid spheres and drops in complex fluids have attracted significant attention from the fluid mechanics community due to their relevance in several natural, industrial, and biological processes, such as fracturing [1], sorting cells and particles [2,3], 4D printing [4], active fluids [5], isolating cells from blood [6,7], clay [8], flow of debris and lava [9], food processing [10] and paint industries [11]. Investigations of single and pair-particle dynamics have been critical in understanding the rich behaviors of such suspensions and emulsions [12–15]. Recently, we studied shear-induced pair interactions between viscous drops in a viscoelastic liquid. Here, we extend it to a shear-thinning viscoelastic liquid, showing that shear-thinning introduces a new reversed pair trajectory.

In Stokes flow, due to its reversibility, two spheres in unbounded shear collide and pass to travel along their original streamlines after collision unless the reversal symmetry is broken by one of the many factors, such as deformability [16], particle roughness [17], inertia [18,19] and viscoelasticity [20]. Following the pioneering work of Batchelor and Green [21] on shear-induced pair-interactions between rigid spheres in viscous fluids, experiments exhibited reversible passing trajectories for most cases except when they are too close and form a doublet rotating/tumbling around each other [22]. For deformable drops in an unconfined shear flow, drops undergo only passing trajectories in the Stokes flow limit. The drop deformability, however, breaks the reversal symmetry, post-collision drops (in contrast to rigid spheres) assume different streamlines, increasing their separation, which in an emulsion leads to shear-induced diffusivity [16,23–25].

Confinement drastically changes the pair trajectories of rigid particles. Zurita-Gotor et al [26] found that confining walls make a rigid particle pair get close to each other, swap vertical positions, and separate without passing in a reversed or swapping trajectory. A similar reversed trajectory in the presence of confinement was also seen for viscous drops by Sarkar et al [27] in negligible inertia, where particles collide and reverse direction; furthermore, they experience a wall-induced lift, moving them to be aligned along the center line. On the other hand, in the presence of inertia, the symmetry of the streamline is broken both for rigid spheres and viscous drops; one observes

* Corresponding Author: Kausik Sarkar, Department of Mechanical and Aerospace Engineering, George Washington University 801 22nd Street NW 10 Washington, DC 20052.
E-mail address: Sarkar@gwu.edu (K. Sarkar).

https://doi.org/10.1016/j.jnnfm.2025.105454
Received 21 April 2025; Received in revised form 12 June 2025; Accepted 13 June 2025
Available online 22 June 2025

passing and reversed trajectories [26–28]. Olapade et al [29], Singh and Sarkar [30], and Chen et al [31] computed passing and reversed trajectories for viscous drop pair in a viscous liquid as a function of Reynolds number, Capillary number, and viscosity ratio.

Rigid particle interactions have also been extensively studied in viscoelastic fluids [32–38] but mostly in a strongly confined domain, which, as noted above have strong effects on particle trajectories. Depending on confinement, they showed reversed (also called 'return'), tumbling or passing trajectories [34,36]. Similar to the viscous case, deformable drops in a viscoelastic matrix introduce additional complexities, not yet adequately investigated. Aggarwal and Sarkar [39] and Guido et al [40] found that the deformation of a viscous drop under shear is non-monotonically affected by the viscoelasticity of the surrounding fluid, which in turn influences their pair trajectory. However, pair interactions between drops in a viscoelastic system haven't been studied much. Recently, our group [41] investigated the pair interactions of two viscous drops in a constant viscosity viscoelastic liquid under shear with negligible inertia and obtained passing and tumbling trajectories. Stiffer drops and increased viscoelasticity favor tumbling trajectory: the critical value of the Weissenberg number for the transition from passing to tumbling is lower for lower capillary numbers, *i.e.*, for drops with less deformability.

The shear-thinning property of a fluid, *i.e.*, a decrease of viscosity with increasing shear rate, plays an important role in the 3D printability of bioink [42,43] and presents interesting physical phenomena such as transient friction during pressure wave propagation [44] and recovery decrease [45]. In a shear-thinning viscoelastic fluid, Feng et al [46] through a 2D simulation found shear-thinning and inertia have competing effects on a solid particle moving in a viscoelastic fluid in a Couette or Poiseuille flow. Several experimental studies observed significant effects of shear-thinning on suspensions [47,48]. In shear-induced pair interactions, spheres in a shear-thinning viscoelastic fluid displayed reversed trajectories on limited occasions [20]. We found one numerical investigation of pairwise interactions of viscous drops in a shear-thinning inelastic (Carreau-Yasuda) fluid. In contrast to the results below, it observed only passing trajectories using a limited variation of the shear-thinning parameter and a relatively large capillary number of 0.1 [49].

Despite the growing interest in pair interactions, the dual influence of viscoelasticity and shear-thinning on the pair interactions between drops has not been widely investigated [12–14,32,41,49]. Here, we numerically study the shear-induced pair interactions of viscous drops in a viscoelastic shear-thinning matrix in an unconfined shear. The mathematical formulation and problem setup are described in Sections 2 and 3. Section 4 discusses the results. Section 5 offers a summary.

2. Mathematical equations and numerical implementation

The mathematical formulation for simulating drops in a matrix for both viscous and viscoelastic fluids has been described in detail in our previous publications [39,50]. Here, a brief overview is provided for completeness. A single-fluid formulation of the drops-matrix system is considered in the entire computational domain Ω (a box of dimensions $L_x \times L_y \times L_z$):

$$\frac{\partial(\rho \boldsymbol{u})}{\partial t} + \nabla\cdot(\rho \boldsymbol{u}\boldsymbol{u}) = \nabla\cdot\tau - \int_{\partial B} d\boldsymbol{x}_B \kappa \boldsymbol{n} \Gamma \delta(\boldsymbol{x} - \boldsymbol{x}_B) \tag{1}$$

$$\nabla\cdot\mathbf{u} = 0 \tag{2}$$

The total stress $\boldsymbol{\tau}$ in general is decomposed into pressure, polymeric (absent in a viscous medium), and viscous parts,

$$\boldsymbol{\tau} = -p\mathbf{I} + \mathbf{T}^p + \mathbf{T}^v, \quad \mathbf{T}^v = \mu_s \mathbf{D}, \tag{3}$$

where ρ is the density, p the pressure, μ_s the solvent viscosity, and $\mathbf{D} = \nabla\mathbf{u} + (\nabla\mathbf{u})^T$ is twice the deformation rate tensor. The superscript T represents the transpose. $\mathbf{T}^p$ is the viscoelastic stress due to the presence of polymer. Γ is the interfacial tension (constant), ∂B represents the surface of the drop consisting of points $\mathbf{x}_B$, κ is the local curvature, $\mathbf{n}$ the outward normal vector to the surface, and $\delta(\boldsymbol{x} - \boldsymbol{x}_B)$ is the three-dimensional Dirac delta function. We employed the FENE-MCR (finite extensible nonlinear elastic modified Chillicot Rallison) model [51] to characterize the viscoelastic behavior of the liquid outside the drops, as in our recent publications [41,52,53]. The FENE-MCR model can be derived from the FENE-CR constitutive equation with conformation tensor **A**:

$$\frac{\partial \mathbf{A}}{\partial t} + \mathbf{u}\cdot\nabla\mathbf{A} = \nabla\mathbf{u}\cdot\mathbf{A} + \mathbf{A}\cdot(\nabla\mathbf{u})^T - \frac{f}{\lambda}(\mathbf{A} - \mathbf{I}), \tag{4}$$

where $\mathbf{A} = \lambda\mathbf{T}^p/\left(\mu_p f\right) + \mathbf{I}$, $f = \left(L^2 + \lambda\left(\sum T^p_{ii}\right)/\mu_p\right)/\left(L^2 - 3\right)$, μ_p is the polymeric viscosity, λ is the relaxation time, and L is the finite extensibility. If L is infinite, which makes $f = 1$, we can get the Oldroyd-B equation. In our simulation, L=*20* is used for the FENE-CR model (shown in previous studies to be sufficient; a further increase of L doesn't change results [53]). The total viscosity for the viscoelastic fluid is $\mu = \mu_s + \mu_p$ (for viscous fluid μ_p=0). As has been shown in our previous publication [41], appropriate approximations lead to the modified FENE-CR equation:

$$\frac{\partial \mathbf{T}^p}{\partial t} + \left\{\mathbf{u}\cdot\nabla\mathbf{T}^p - \nabla\mathbf{u}\cdot\mathbf{T}^p - \mathbf{T}^p\cdot\nabla\mathbf{u}^T\right\} + \frac{f}{\lambda}\mathbf{T}^p = \frac{f}{\lambda}\mu_p\mathbf{D}, \tag{5}$$

which upon elastic viscous splitting [54] obtains for $\mathbf{T}^p$ at n+1 time step as

$$\begin{aligned}(\mathbf{T}^p)^{n+1} \quad &= \left[(\mathbf{T}^p)^n - \left(\mu_p\mathbf{D}\right)^n\right]e^{-(f/\lambda)\Delta t} + \left(\mu_p\mathbf{D}\right)^n \\ &-\frac{\lambda}{f}\left[\mathbf{u}\cdot\nabla\mathbf{T}^p - \nabla\mathbf{u}\cdot\mathbf{T}^p - \mathbf{T}^p\cdot\nabla\mathbf{u}^T\right]^n\left[1 - e^{-(f/\lambda)\Delta t}\right]\end{aligned} \tag{6}$$

We use a front-tracking method [55] to track the two drops' location. An alternating direction implicit (ADI) method is employed to alleviate the time step limitations. The model and its numerical implementation have been extensively validated in previous articles [50,53,56]. The FENE-MCR model has been extensively used in modeling different viscoelastic flows [57–60].

In this paper, we simulate viscous drops in a shear-thinning viscoelastic surrounding liquid. To model the shear-thinning behavior of the matrix liquid, we used a power-law model of shear-thinning [42,61–65] for the viscosity $\mu(\dot{\gamma})$ in a range $[\dot{\gamma}_l, \dot{\gamma}_u]$ limited by a lower and a higher constant viscosity values outside the range:

$$\mu(\dot{\gamma}) = \begin{cases} \mu_0, & \dot{\gamma} \le \dot{\gamma}_l \\ \mu_0(\dot{\gamma}/\dot{\gamma}_l)^{n-1}, & \dot{\gamma}_l < \dot{\gamma} \le \dot{\gamma}_u \\ \mu_0/100, & \dot{\gamma} > \dot{\gamma}_u \end{cases} \tag{7}$$

where μ_0 is zero shear rate viscosity. $\dot{\gamma} = \sqrt{\mathbf{D}:\mathbf{D}}$ is the local shear rate, $\dot{\gamma}_l$ is the lower shear rate limit, and $\dot{\gamma}_u = \dot{\gamma}_l 100^{1/1-n}$ is the upper shear rate limit. Fig. 1(a) shows the curve of viscosity at n=0.5. At $n = 1$, the matrix fluid is a Boger fluid with a fixed viscosity μ_0. As in our previous studies, we choose the simplest constitutive model acknowledging the complexity of real polymeric liquids. We feel that such an approach is sufficient for the present problem, where the purpose is to understand the fundamental physics underlying the model problem. Note that the shear-thinning viscoelastic model adopted here is different from the White Metzner model [66], where a shear rate dependent relaxation time $\lambda(\dot{\gamma}) = \mu(\dot{\gamma})/G_0$ is used with a constant shear modulus G_0. Unlike the White-Metzner model, the shear-thinning Oldroyd B type model with an independent relaxation time, used here as well as by others [46], allows a global Weissenberg number *Wi* separating the shear-thinning effects from viscoelastic ones. Also, note that the White-Metzner model doesn't satisfy the Lodge-Meissner relationship [11]. In any event, physics of the

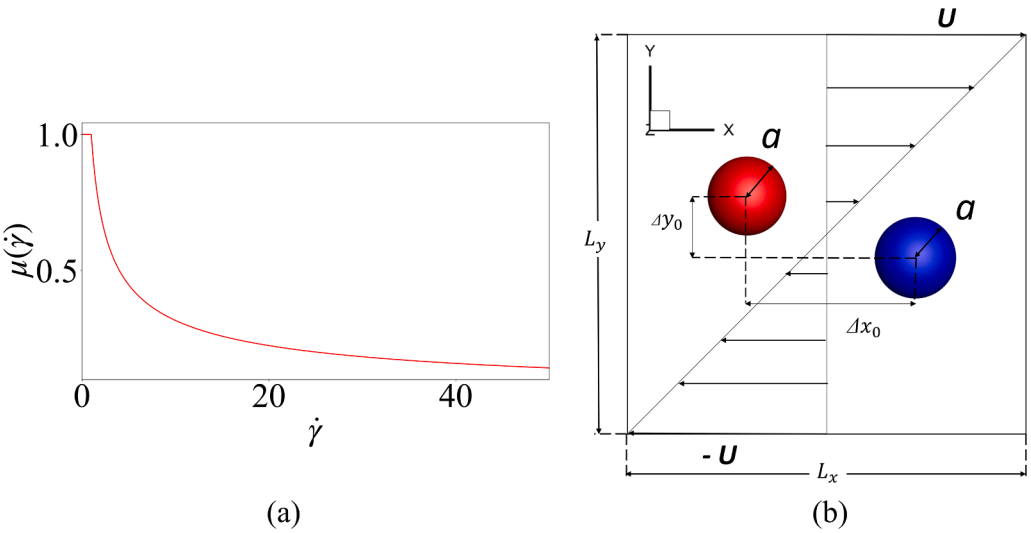

Fig. 1. (a) Shear-thinning viscosity at n=0.5 (b) Schematic of the problem with the initial separations of two drops in a shear flow.

model chosen here is similar to that of the White-Metzner model with a quantitative difference (in the values of the parameters describing transitions between different trajectories Figs. 6 and 12) due to the simultaneous lessening of viscoelastic effects with shear-thinning.

3. Problem setup

Two spherical drops with equal radius a are located at the center of the rectangular computation domain (Fig. 1b). The initial separations between drops are chosen as Δx_0=*2.5a* in x direction, Δy_0=*0.25a* in the y-direction, and Δz_0=*0* in the z-direction (except in a later section where the effects of initial separation are briefly studied). The domain size is $L_x = 30a$, $L_y = 30a$, $L_z = 5a$ and is discretized with 384 × 384 × 64 grid points along the x, y, z directions, respectively. A shear flow is generated by moving the top and the bottom wall with velocities U and $-U$, resulting in a global shear rate of $\dot{\gamma}_1 = 2U/L_y$. The drop radius a and the inverse shear rate ${\dot{\gamma}_1}^{-1}$ serve as the length and the time scales, respectively, leading to $\mathrm{Re} = \rho_m \dot{\gamma}_1 a^2/\mu_{m0}$, capillary number $Ca = \mu_{m0}\dot{\gamma}_1 a\ /\Gamma$ and Weissenberg number, $Wi = \lambda\dot{\gamma}_1$ as the leading defining nondimensional parameters. ρ_m is the density of the matrix and μ_{m0} is the zero-shear rate viscosity of the matrix. The subscripts m and d refer to matrix and the drop fluid respectively. As noted before, the drop is a constant viscosity Newtonian liquid. The other nondimensional parameters of the problem are viscosity ratio $\lambda_\mu = \mu_d/\mu_m$, the ratio of the polymeric viscosity of the matrix to the total matrix viscosity $\beta = \mu_{pm}/\mu_m$ and shear-thinning parameters—the power law index n and the nondimensional lower shear rate $\dot{\gamma}_l/\dot{\gamma}_1$. We choose $\dot{\gamma}_l/\dot{\gamma}_1 = 1$, *i.e.*, the shear-thinning is triggered above $\dot{\gamma}_1$. Because of the explicit nature of the code and the resulting time step limitation, the Reynolds number is set at 0.01 as a proxy for Stokes flow. In view of the large number of parameters in this problem and our computational resources, we restrict our study to a viscosity-matched system ($\lambda_\mu = 1$) except in Section 4.4.3 where the effects of viscosity ratio variation are studied. We also consider equal contributions of polymeric and solvent viscosities ($\beta = 0.5$) in the matrix medium. We have previously investigated the effects of viscosity ratio and initial drop positions with expected results: increasing separations decreases interactions [29,30,41], and increasing β increases the effect of viscoelasticity. Previous publications in our group established that the domain sizes $L_x = 30a$, $L_y = 30a$, $L_z = 5a$ with 384 × 384 × 64 grid points along x, y, and z directions are sufficient for the study of pair interaction and avoiding the boundary effects. Note that the code has been extensively investigated for domain and grid convergence [29,67], showing that larger domain sizes and smaller grids lead to insignificant changes. Pair interactions between drops in a viscoelastic system haven't been studied before. However, we successfully compared with previous experiments by Guido and Simeone [68] and boundary element simulations by Lac et al [69] of pair-interactions in a viscous system. Below, we first study the effects of shear-thinning in a viscous matrix and then in a viscoelastic matrix.

4. Results and discussion

To study the effects of shear-thinning, we vary n in the range between 0.1 and 1 (constant viscosity). Experimentally, the concentration of anionic polyacrylamide polymer (PAAm) was varied in water to obtain different n obtaining a minimum value of 0.08 [47,70]. In natural and industrial viscoelastic flows, the strength of elasticity (Wi) varies widely. We have chosen to vary it in a limited range (≤ 2) to avoid the well-known high Weissenberg numerical problem. However, we feel that the study adequately describes the underlying physics.

4.1. Viscosity field in a shear-thinning viscous medium around a viscous drop in shear

We briefly see the effects of shear-thinning around a single drop in a shear flow in Fig. 2. It shows the contours of shear rate and viscosity for different n for a single drop in a viscous liquid. The shear rate distributions are as expected with a higher value near the drop (Figs. 2a, b, c); it aligns with the results in the article [38]. For the constant viscosity case, the viscosity is matched (Fig. 2d). As we increase shear-thinning, locally viscosity reduces in the high shear rate region near the drop from the n=0.5 case (Fig. 2e) to the n=0.1 case (Fig. 2f). Note the increase in local shear rate near the drop with increasing shear-thinning (Figs. 2a, b, c) to compensate for the decrease in viscosity keeping a stress balance.

4.2. Three trajectories: passing, reversed, and tumbling

The system is characterized by many parameters, Ca, n, Wi. In the sections below we vary them systematically, to find three different trajectories for the drop pairs in this article (Fig. 3): passing, reversed, and tumbling. Note that the pair-interaction of drops in a constant viscosity Newtonian system shows only a passing trajectory. In a passing trajectory, drops or particles approach in the compression quadrant and then slide past each other in the separation quadrant along a streamline parallelly shifted from the original streamline (Fig. 3a). It leads to shear-induced diffusion [24,25,71,72] and enhanced mixing. In a reversed

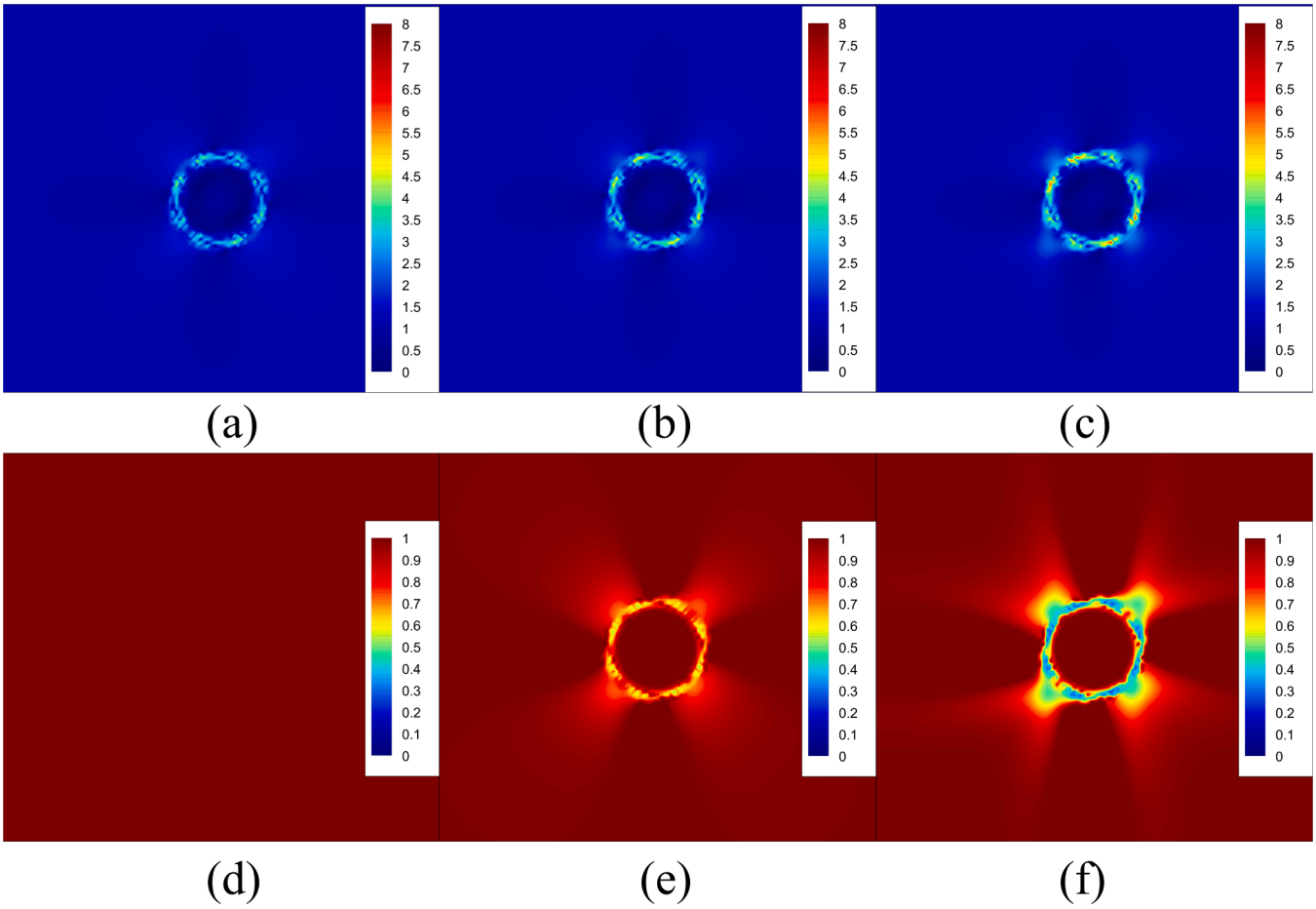

Fig. 2. The contour of shear rate and corresponding viscosity in the domain at Wi=0 and Ca=0.01 (a) shear rate at n=1 (b) shear rate at n=0.5 (c) shear rate at n=0.1 (d) viscosity at n=1 (e) viscosity at n=*0.5* (f) viscosity at n=0.1.

trajectory—seen before for drops at finite Reynolds numbers [29,30], for rigid spheres in confined Stokes flow (called swapping trajectories [26]), and in a viscoelastic shear-thinning liquid [20]—particles upon approach reverse direction and move backward (Fig. 3b). In a tumbling trajectory, seen in viscoelastic fluid [41], drops don't separate and rotate around each other after the collision (Fig. 3c).

4.3. *Pair-interactions in a viscous matrix*

4.3.1. *Effects of shear-thinning*

Before we investigate the effects of shear-thinning on pair interactions between viscous drops in a viscoelastic matrix, we investigate them in a viscous matrix ($Wi = 0$) which has not been studied before. We take two cases of Ca, one smaller (Ca=0.01) and therefore less deformable than the other case (Ca=0.2) noting the important effect that Capillary number plays in drop dynamics, namely the deformability [27,29,30,41,49]. Both for Ca= 0.01 (Fig. 4a) and Ca = 0.2 (Fig. 4b), we note a passing trajectory for the constant viscosity case (n=1). Upon decreasing the power law index n the trajectories progressively change but always are passing for the more deformable Ca= 0.2. However, for Ca = 0.01, they eventually transition into the reversed type for n= 0.1. For the passing trajectories, decreasing n brings the drops closer to each other (absolute values of $\Delta x/a$ and $\Delta y/a$ decreasing) during their approach in the compression quadrant. Fig. 4(c) plots $(\Delta y - \Delta y_0)/a$ as a function of time for Ca = 0.01 to demonstrate the closer approach over a longer time duration. In the region between the approaching drops, the rapid spatial change in velocity, *i.e.*, the shear rate, reduces the viscosity leading to a closer approach. Decreasing n for passing trajectories also increases the final $\Delta y/a$, *i.e.* interaction-induced cross-stream displacement of the drops, which is critical for mixing of shear-induced diffusion [16]. In Fig. 4(d), we plot the final $(\Delta y - \Delta y_0)/a$ for the passing trajectories as a function of n for different Ca. We note that for a particular capillary number, increasing n decreases net cross-stream separation, and thereby shear-induced diffusion. However, note that for a specific value of n, there is a non-monotonic variation with Ca, as was also observed in the boundary element simulation of non-shear-thinning pair-interaction by Loewenberg and Hinch [16] (Fig. 5 in that article). This has resulted in non-monotonic variation in shear-induced diffusivity with Ca seen in our recent investigation [23]. The non-monotonicity results from the competition between increasing deformation (at lower Ca leading to stronger interactions and larger cross-stream separation) and decreasing inclination (at higher Ca leading to easier passing and lower cross-stream separation) with capillary number.

4.3.2. *Physics of trajectories and phase plot in n-Ca for the viscous matrix case*

To understand the physics behind the transition from passing to reversed trajectories caused by shear-thinning, we plot the streamlines around a single drop in a shear flow after a steady state has been reached (Fig. 5). Even though the pair dynamics of drops are a result of the interactions between them, and the presence of the second drop changes the flow field, the flow field around a single drop offers an approximate physical explanation of the pair trajectories. The parameters for Fig. 5(a) and (b) correspond to passing and reversed trajectories, respectively at Ca= 0.01. Compared to the constant viscosity case (Fig. 5a) with mostly

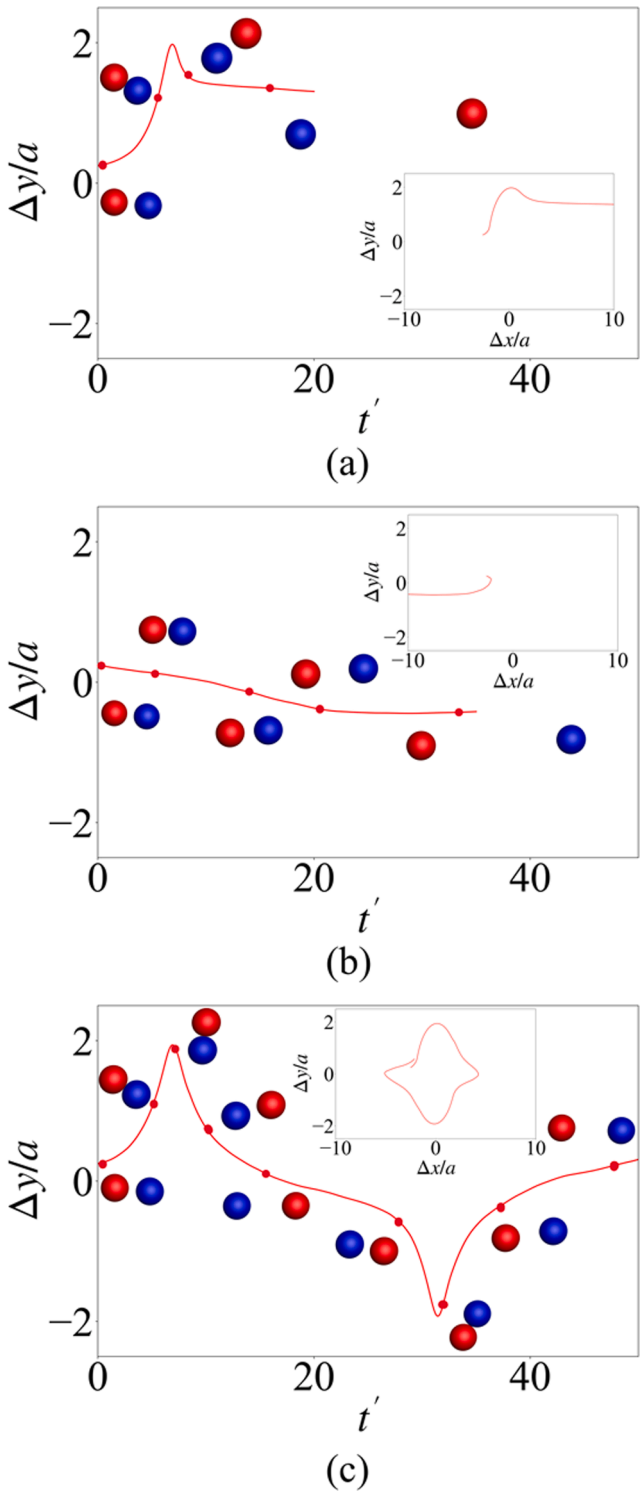

Fig. 3. Drop interaction snapshots at different simulation times along with their cross-stream separation at Ca=0.01 (a) passing trajectory at Wi=0, n=1 (b) reversed trajectory at Wi=0, n=0.25 (c) tumbling trajectory at Wi=1.2, n=1. Insets show the relative trajectories of drops $\Delta y/a$ *vs.* $\Delta x/a$.

passing streamlines, shear-thinning introduces a large region of reversed streamlines in Fig. 5(b), which in pair interaction captures the second drop in a reversed trajectory. Fig. 5(c) shows that for a more deformable drop (Ca=0.2), the region of reversed streamlines becomes smaller due to the decreased opposition to the imposed flow, leading to an eventual passing trajectory in pair interactions. The more deformed shapes [50, 73] of these deformable drops facilitate them to slide past each other.

The transition from a passing to a reversed trajectory has also been observed in the previous study of pairwise interaction under shear in a constant-viscosity medium by Olapade et al [29] in the presence of inertia. They noted that increasing capillary number (Ca) induces two effects: firstly, the drops experience less opposing force, and secondly, a portion of the more deformed drop reaches the region with reversed streamlines. The interplay between these effects ultimately determines the type of trajectory observed, as is also the case here in Figs. 5 (a) and (b). Unlike in our previous study in the presence of inertia, here the reversed streamlines around the drop (Fig. 5) are caused by shear-thinning.

In Fig. 5, we also show the pressure for all three cases. Note that according to the equation of motion in the Stokes limit:

$$\partial_i[\mu(\dot{\gamma})\partial_i]v_j = \partial_j p, \tag{8}$$

a weighted Laplacian of the velocity component v_j is approximately related to the pressure gradient (normal to the pressure contour shown), at least in a local shear flow approximation. We note that the Stokes Eq. (8) is elliptic, with pressure and velocity both being dependent variables to be simultaneously determined by the boundary value problem. Therefore, the physics of reversed streamlines in the presence of shear-thinning is not amenable to an easy understanding. However, the reversed streamlines in Figs. 5(b) and (c) are associated with the pressure fields in the presence of shear-thinning. The pressure fields here are different from the one in Fig. 5(a) in the absence of shear-thinning, with the lobe structures guiding the streamlines. For the case of the larger Ca =0.2 (Fig. 5c), due to the less rigid drop, the effect on the pressure field is diminished, reducing the extent of the reversed streamline region. This in turn fails to result in a reversed trajectory.

Finally, Fig. 6 shows an n-Ca phase plot based on extensive simulations varying the parameters. It shows that reversed trajectories are restricted to the low n and low Ca region, *i.e.*, high shear-thinning and less deformable drops as a result of the competing dynamics described above.

4.3.3. *Effects of viscosity ratio on pair-interactions*

In this paper, we primarily investigated pair interactions in a viscosity-matched system ($\lambda_\mu = 1$). In this section, we briefly consider the effects of viscosity ratio variation at Ca=0.2, n=0.1, $\Delta x_0 = 2.5a$ and $\Delta y_0 = 0.25a$. Previously, Fig. 4(b) indicated that $\lambda_\mu = 1$ leads to passing trajectories for all n's considered for these parameters. However, Fig. 7 here shows that with varying λ_μ, one gets both passing and reversed trajectories. For the highest $\lambda_\mu = 10$, the trajectory is passing with a minimum final cross-stream relative separation. Note that in absence of shear-thinning, $\lambda_\mu \to \infty$ leads to the reversible rigid sphere limit with no net increase in cross-stream separation. In Fig. 7, as λ_μ decreases, the drops experience closer approaches leading to a larger final cross-stream relative separation. Eventually, the trajectory transitions to reversed for $\lambda_\mu = 0.1$.

4.4. *Pair-interactions in a viscoelastic matrix*

4.4.1. *Effects of shear-thinning in a viscoelastic matrix*

In this section, we discuss the effects of outer fluid elasticity and shear-thinning on the interaction between two drops under shear. Previously [41], we showed that pair interactions in a viscoelastic fluid without shear-thinning result in a transition of passing trajectories into tumbling above a critical value of the Wi, due to the effects of viscoelastic stresses. The effects are more dominant for less deformed drops at lower capillary numbers. The previous section on the viscous case also underscores the fact that the interesting dynamics due to shear-thinning are primarily seen at low capillary numbers. In the interest of brevity, we therefore restrict our viscoelastic simulation to the capillary number of $Ca = 0.01$ and vary Wi in the range 0.1–1.5 and n in 0.1–1 in this section leaving the effects of capillary number variation to the SubSection 4.4.3.

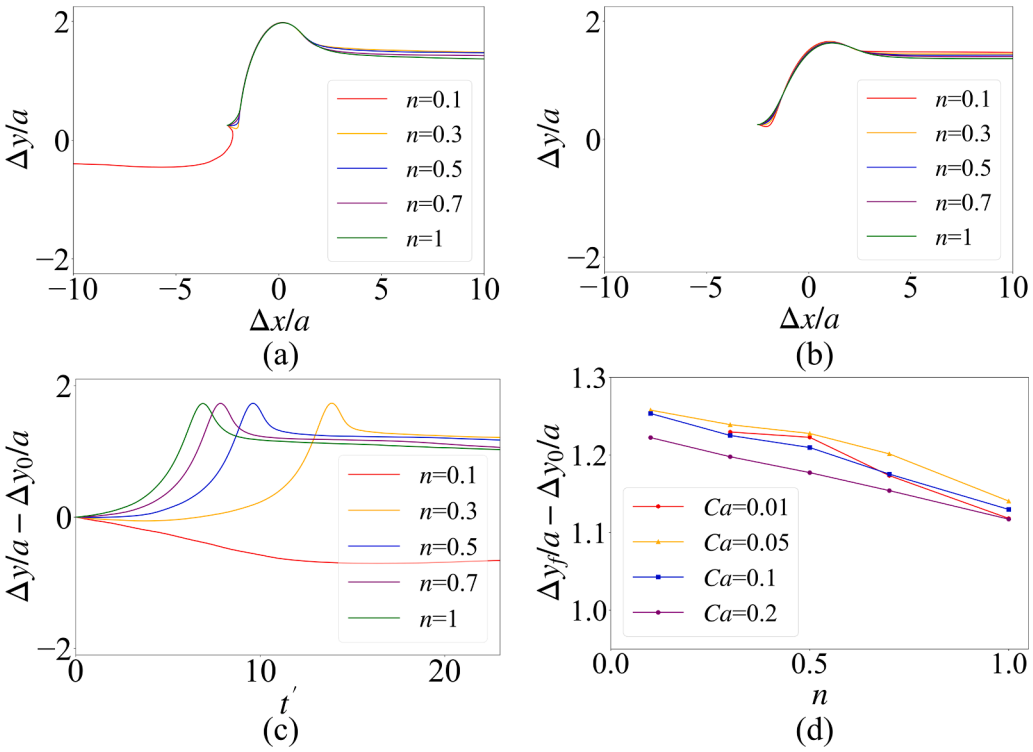

Fig. 4. Effects of shear-thinning on pair interactions in a viscous matrix: (a) Relative trajectories for Ca= 0.01 showing both passing and reversed trajectories. (b) Relative trajectories for Ca = 0.2 showing only passing trajectories; (c) Cross-stream separation relative to its initial value with time for Ca = 0.01 (d) Final cross-stream relative to its initial value separations for passing trajectories for different Ca as a function of n.

The n = 1 case represents non-shear-thinning Boger fluids with varying relaxation times.

In Fig. 8, we consider the relative trajectory of drops for varying n for two different Wi values, with the initial drop separations fixed at Δx_0= 2.5a and Δy_0= 0.25a for all simulations. At Wi=0.2, Fig. 8(a) shows passing trajectories for n>0.25 transitioning to reversed trajectories for n= 0.25 and 0.1. In Fig. 8(b), we see at Wi=1.2 only passing and tumbling trajectories, tumbling for n=0.75, 1 and passing ones for stronger shear-thinning. For passing trajectories, the final cross-stream separation (Δy_f /a) increases with shear-thinning to be discussed in detail below. This demonstrates a significant effect of shear-thinning on drop trajectories.

In Fig. 9(a), we investigate the effects of Wi variation at a fixed n =0.25. It shows all trajectories: reversed for Wi = 0.1, 0.3, passing for Wi = 0.8, 1.2, and finally a tumbling trajectory for Wi = 1.5. We also see for passing trajectories, the post-interaction drop separation decreases with increasing Wi, eventually becoming a tumbling trajectory. At Wi = 1.5, the tumbling trajectory is not symmetric because the drops experience a slight excursion in the z-direction. To understand it better, we show snapshots of the drops at different time instants in Fig. 9(b) with $\Delta z/a$ *vs.* $\Delta x/a$ in its inset. It demonstrates that drops go around each other with a small shift in the z-direction.

Given that the drops are initially positioned at the central plane (z =0), the slight z-shift in approaching the final tumbling trajectory is due to the numerical perturbation breaking the symmetry [18]. Lac et al [74] in their study of pair interactions between capsules in shear, observed that the initial separation in the z-direction leads to a shifting of the passing trajectory in the same direction during the interaction of two capsules in a simple shear flow. The physics at the transition between two different regimes, such as here between passing and the tumbling trajectories, is inherently sensitive to small perturbations, which explains the symmetry breaking and slight traversing of drops in the z-direction seen here. Away from transition, *i.e., Wi* far from the critical value, we didn't observe such symmetry breaking. We have previously studied the effects of the vorticity direction offset on pair interactions [30].

Fig. 10(a) shows the variation in cross-flow separation $\Delta y/a$ between drop centers as a function of time t' at Wi =0.2. Similar to the viscous case (Fig. 4c), decreasing n results in the peak of $\Delta y/a$ appearing later, *i.e.*, a closer approach (also see Fig. 8a) of drops over longer periods for passing trajectories. For n=0.1 and 0.25, one obtains reversed trajectories, with shorter period of interactions for n=0.1. At other Wi numbers, similar trends are observed. This observation suggests that at a specific Wi, as n approaches the critical value for reversed or passing/tumbling trajectories, the drops require a longer time to determine their trajectory selection. Finally, for passing trajectories, we plot the final cross-stream separation relative to their initial separation of drops as a function of n for different Wi (Fig. 10b) as we did in the viscous case. Increasing viscoelasticity decreases the separation (anticipating an approach to tumbling of drops for higher Wi). The shear-thinning reduces this effect, *i.e.*, the relative separation increases with n decreasing from 1. For Wi =1.2 and n =0.25, 0.5, the final cross-stream separations relative to their initial values are negative. Fig. 8(b) shows these cases are close to the transition to tumbling (n=0.75 is a tumbling trajectory) and initially dips down like a tumbling trajectory before separating into a passing trajectory. Note the slight non-monotonicity for Wi =1.0 case going from n=0.1 to 0.25 due to the slight z-shift of the trajectories noted above. Just like in the viscous case, we can conclude that decreasing shear-thinning and increasing viscoelasticity decrease shear-induced diffusion.

4.4.2. *Physics of trajectories and phase plot in n-Wi for the viscoelastic matrix*

To investigate the physics behind the three types of trajectories, Fig. 11 compares the streamlines encompassing a single drop for different Wi and n values. Fig. 11(a) for a strong viscoelastic case of Wi = 1.2 with no shear-thinning (n=1) shows a large region of spiraling streamlines (also seen recently around a sheared soft elastic particle in a

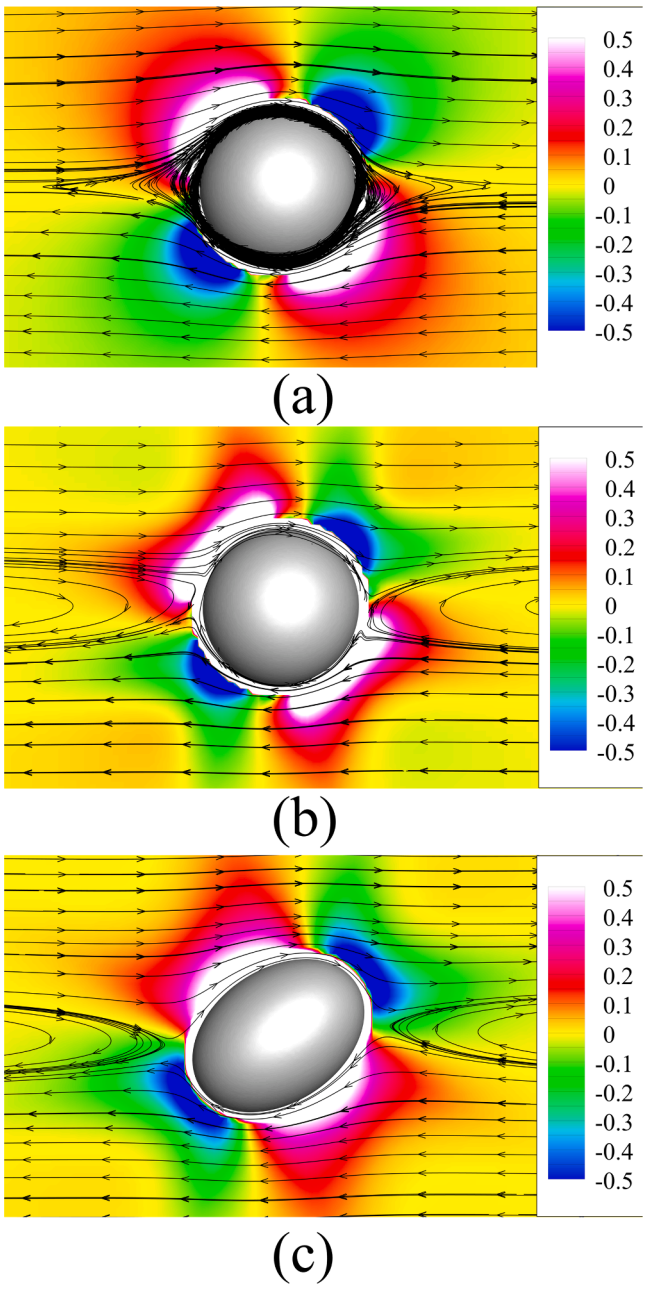

Fig. 5. Streamlines and pressure around a single drop placed at the center of the domain and at Wi=0 (a) n=1, Ca=0.01, (b) n=0.1, Ca=0.01, (c) n=0.1, Ca=0.2.

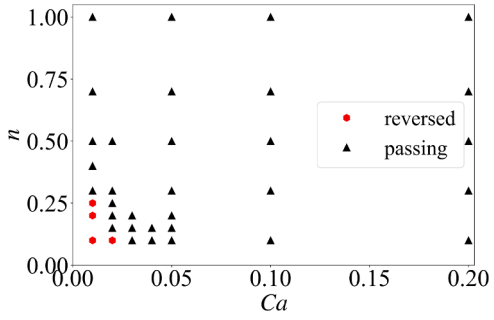

Fig. 6. Phase plot of trajectories as a function of Ca and n.

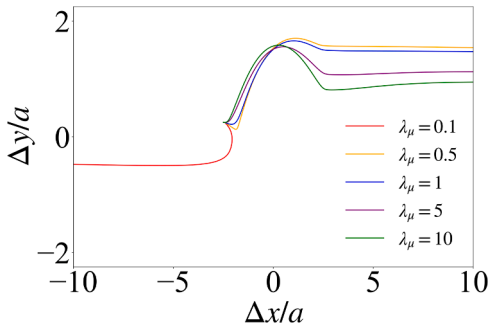

Fig. 7. Relative trajectories of drops for Ca=0.2, n=0.1 at different λ_μ.

viscoelastic medium [75]) that traps a second drop into a tumbling trajectory. Introducing shear-thinning at $n = 0.1$ (Fig. 11b) results in reverse streamlines, reducing considerably the region of spiraling streamlines and thereby the possibility of a tumbling trajectory, which in effect leads to a passing trajectory for these parameter values. As shown in our previous article [41] the normal stress differences in the viscoelastic medium, specifically the hoop stress around the curved streamlines, are what result in the region of spiraling streamlines. Therefore, reducing Wi to 0.2 in Figs. 11(c) and (d) drastically reduces the region of spiraling streamlines. For the case without shear-thinning (Fig. 11c), it leads to a passing trajectory. In Fig. 11(d), the combined effect of shear-thinning ($n = 0.1$) and reduced viscoelasticity generates a strong region of reversed streamlines without any spiraling region and results in a reversed trajectory. Please note that the results match the findings of the experimental observations of pair interactions between spheres [20], where reversed trajectories were seen in shear-thinning matrices (worm-like micellar solution and a broad-spectrum shear--thinning elastic polymer solution), but not in constant-viscosity liquids (a reference Newtonian fluid and a high elasticity Boger fluid).

Fig. 12 shows all three types of trajectories in a Wi-n phase plot obtained by exploring the parameter space by extensive simulation. Reversed trajectories are favored by shear-thinning (small n). Tumbling trajectories are a result of matrix viscoelasticity giving rise to a large region of spiraling streamlines. The phase plot describes a competition between the two with reversed trajectories at the lower left corner (strong shear-thinning and low viscoelasticity) of the phase plot going over to tumbling trajectories at the upper right region (less shear-thinning and strong viscoelasticity), separated by a region of passing trajectories. As Wi increases, the critical value of n for transition between reversed and passing trajectories decreases, *i.e.*, more shear-thinning is warranted to counter the effects of increased viscoelasticity. Our exploration of the parameter space has been limited by computational resources, keeping the total computational time of the simulation within a reasonable limit. We find no reversed trajectories for $Wi \geq 0.5$ and similarly, no tumbling trajectories $Wi \leq 1.0$.

For $Wi = 1.1$, tumbling occurs only for $n \geq 0.75$ with passing trajectories below this value. With increasing Wi, the transition from tumbling to passing occurs at lower and lower n. For $Wi = 1.5$, all trajectories are tumbling for all n (considered here ≥ 0.1). At $Wi = 0.4$ and below, reversed trajectories appear, but they are absent for $n \geq 0.3$. The critical value for transitions between reversed and passing trajectories remains between 0.25 and 0.3. From the phase plot, we note that although the cases of Wi =0.4, n=0.2 and Wi=0.5, n=0.1, present passing trajectories, they take an extraordinarily long time—50 inverse shear units—when the crossflow separation ($\Delta y/a$) remains unchanged before a clear preference for one of the trajectories can be identified. Choi et al. also saw a similar phenomenon for rigid particles in a confined viscoelastic flow in that between the transition from reversed to passing trajectories, particles remained at fixed positions [35]. This indicates the typical behavior near a transition point defined by a delicate balance between the competing dynamics [30].

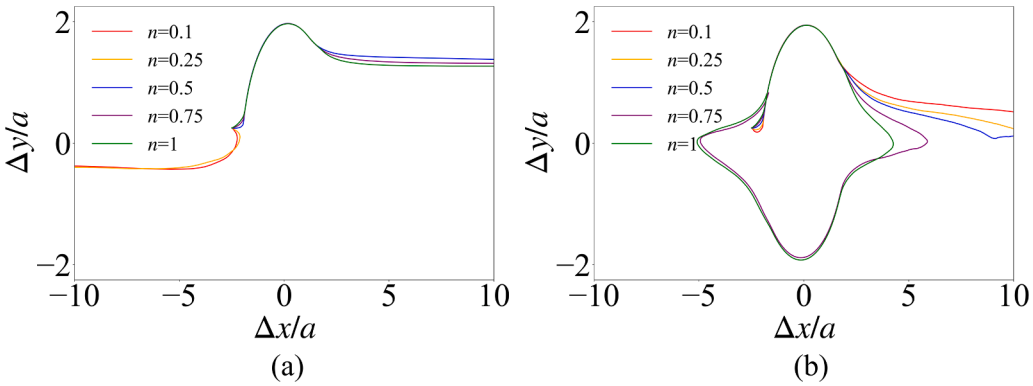

Fig. 8. Relative trajectories of drops for Ca=0.01 (a) Wi=0.2 at different n (b) Wi=1.2 at different n.

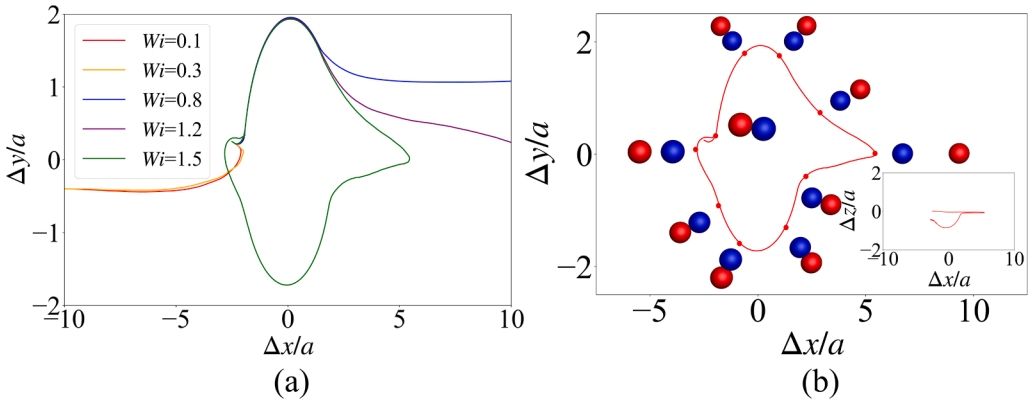

Fig. 9. Relative trajectories of drops (a) at Ca = 0.01, n = 0.25 for different Wi. (b) Relative position along with drop snapshots at different positions at n=*0.25*, Wi=*1.5*. Inset of (b) shows the relative trajectories of drops, $\Delta z/a$ *vs.* $\Delta x/a$.

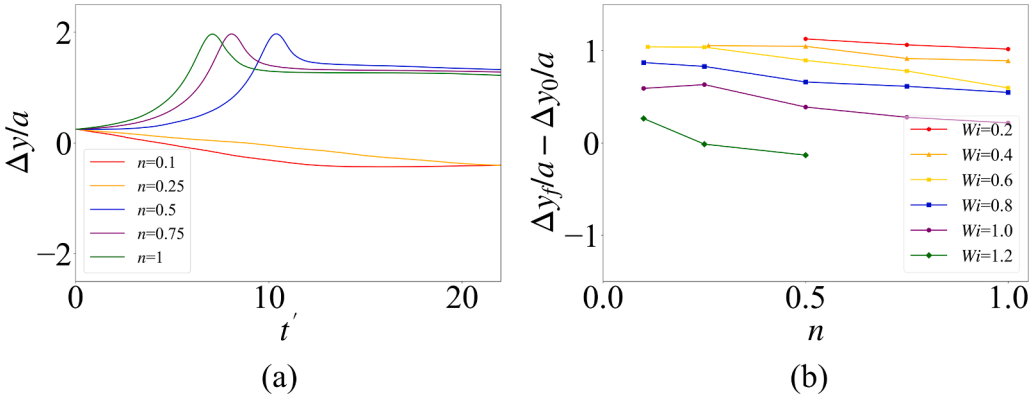

Fig. 10. Plots of (a) $\Delta y/a$ with t' at Ca=0.01, Wi=0.2 at different n. (b) $(\Delta y_f - \Delta y_0)/a$ at Ca=0.01, at different Wi and n.

4.4.3. *Effects of Ca variations*

After discussing the drops' interactions at a low capillary number of Ca=0.01, here we briefly consider the effects of Ca variation at a fixed Weissenberg number of Wi =1.2. Fig. 13(a) shows that more deformable drops (Ca=0.1) result in passing trajectories for all n. Increasing shear-thinning increases net cross-stream separation. Fig. 13(b) describes the effects of capillary number variation at n=0.75: while the least deformable drop (Ca=0.01) results in a tumbling trajectory due to the more prominent spiraling streamlines around a single drop (as discussed before), higher capillary numbers result in passing trajectories due to the increased deformation facilitating sliding of drops.

4.4.4. *Effects of initial drop separation*

In previous sections, we fixed the initial y separation at Δy_0=*0.25a*. In Fig. 14, we briefly examine the effects of varying the initial y separation at Wi=1.2, Ca=0.01, n=0.75. For smaller initial y separations (Δy_0=0.125*a*, 0.25*a* and 0.75*a*), drops obtain tumbling trajectories because of the region of spiral streamlines trapping the second drop. However, when the initial y separation is large enough (Δy_0=1*a* and 1.25*a*), the second drop escapes the region of spiral streamlines leading to a passing trajectory.

5. Summary

We performed a detailed numerical investigation of the effects of

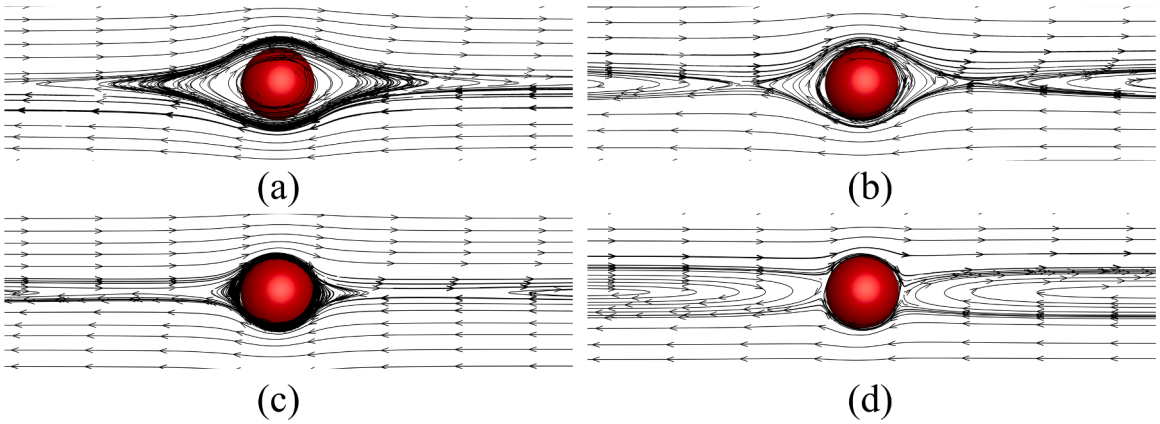

Fig. 11. Streamlines around a single drop placed at the center of the domain at (a) n=1, Wi=1.2, (b) n=0.1, Wi=1.2, (c) n=1, Wi=0.2, and (d) n=0.1, Wi=0.2.

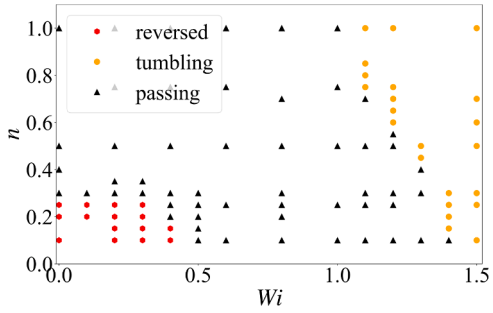

Fig. 12. Phase plot of trajectories as a function of Wi and n at Ca=0.01.

matrix shear-thinning on shear-induced pair interactions between two equal-sized viscous drops in viscous and viscoelastic media. Note that previous studies of pair interactions in a viscoelastic system have been primarily restricted to rigid particles in a confined geometry. Here, we show that shear-thinning in a viscous or a viscoelastic matrix introduces a new reversed trajectory, which was seen before only in the presence of confinement or inertia. In the case of a viscous matrix, we see passing trajectories encountered in constant viscosity fluid, where the drops after interaction pass each other and separate in the extension quadrant, experiencing a shift in the cross-stream direction. Increasing shear-thinning (power law index n less than 1) eventually leads to a reversed trajectory for less deformable drops (small capillary numbers). The effects are seen as a result of reversed streamlines observed around a single drop in a shear flow in a shear-thinning liquid. We have offered a simple explanation for the reversed streamlines in terms of the pressure gradient around a drop in the presence of shear-thinning. Simulations with varying parameters describe the regions of different trajectories in the n-Ca phase plot, with reversed trajectories restricted to small n and small Ca.

Extending the investigation to a shear-thinning viscoelastic matrix, we observe a third trajectory, tumbling, seen before in our recent study of constant viscosity viscoelastic systems [41]. Matrix viscoelasticity introduces a region of spiraling streamlines due to the hoop stresses along the curved streamlines around a single drop, which eventually traps a second drop in a tumbling trajectory. Performing simulations varying n and Weissenberg number, we obtain a phase plot in the n-Wi space showing reversed trajectories for strong shear-thinning (small n) and low viscoelasticity (low Wi) and tumbling trajectories for low shear-thinning and strong viscoelasticity, with a region of passing trajectories for intermediate values of n and Wi. The study has explored the effects of shear-thinning on pair interactions in unconfined shear. It observed three different trajectories depending on the parameters

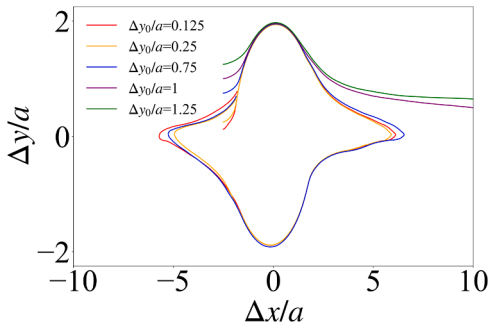

Fig. 14. Relative trajectories of drops at Wi=1.2, Ca=0.01, n=0.75, at different $\Delta y_0/a$.

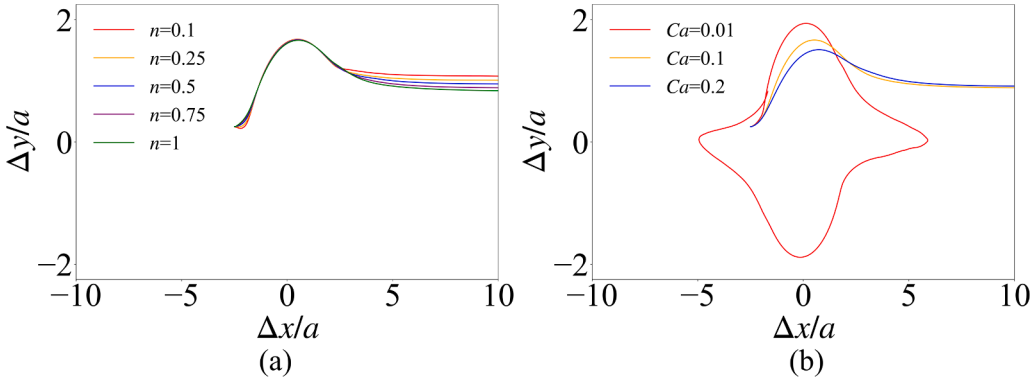

Fig. 13. Relative trajectories of drops at Wi=1.2 (a) Ca=0.1, at different n (b) n=0.75, at different Ca.

defining the underlying physics and offered insights into viscous and viscoelastic shear-thinning emulsions.

CRediT authorship contribution statement

Haoqian Wang: Writing – original draft, Visualization, Validation, Methodology, Investigation, Formal analysis, Data curation, Conceptualization. **Anik Tarafder:** Software, Resources. **Kausik Sarkar:** Writing – review & editing, Supervision, Software, Resources, Project administration, Methodology, Investigation, Funding acquisition, Formal analysis, Conceptualization.

Declaration of competing interest

The authors declare that they have no known competing financial interests or personal relationships that could have appeared to influence the work reported in this paper.

Acknowledgment

K.S. acknowledges partial support from the National Science Foundation Award 1239105. The authors acknowledge time on the Pegasus cluster at GWU.

Data availability

The data sets generated and/or analyzed during the current study are available from the corresponding author upon reasonable request.

References

[1] A.C. Barbati, J. Desroches, A. Robisson, G.H. McKinley, Complex fluids and hydraulic fracturing, Annu. Rev. Chem. Biomol. Eng. 7 (2016) 415–453, https://doi.org/10.1146/annurev-chembioeng-080615-033630.
[2] P. Sajeesh, A.K. Sen, Particle separation and sorting in microfluidic devices: a review, Microfluid Nanofluid 17 (2014) 1–52, https://doi.org/10.1007/s10404-013-1291-9.
[3] J. Zhou, I. Papautsky, Viscoelastic microfluidics: progress and challenges, Microsyst. Nanoeng. 6 (2020) 113, https://doi.org/10.1038/s41378-020-00218-x.
[4] S. Guo, H. Cui, T. Agarwal, L.G. Zhang, Nanomaterials in 4D printing: expanding the frontiers of advanced manufacturing, Small 20 (2024) 2307750, https://doi.org/10.1002/smll.202307750.
[5] D. Saintillan, Rheology of active fluids, Annu. Rev. Fluid Mech. 50 (2018) 563–592, https://doi.org/10.1146/annurev-fluid-010816-060049.
[6] J. Zhou, C. Tu, Y. Liang, B. Huang, Y. Fang, X. Liang, I. Papautsky, X. Ye, Microfluidic separation of particles from whole blood using shear induced diffusion, Microfluidics, BioMEMS, and Medical Microsystems XV, SPIE, 2017, pp. 148–154.
[7] J. Zhou, C. Tu, Y. Liang, B. Huang, Y. Fang, X. Liang, I. Papautsky, X. Ye, Isolation of cells from whole blood using shear-induced diffusion, Sci. Rep. 8 (2018) 9411, https://doi.org/10.1038/s41598-018-27779-2.
[8] C. Ancey, H. Jorrot, Yield stress for particle suspensions within a clay dispersion, J. Rheol. (N N Y) 45 (2001) 297–319, https://doi.org/10.1122/1.1343879.
[9] G. Ovarlez, F. Mahaut, S. Deboeuf, N. Lenoir, S. Hormozi, X. Chateau, Flows of suspensions of particles in yield stress fluids, J. Rheol. (N N Y) 59 (2015) 1449–1486, https://doi.org/10.1122/1.4934363.
[10] S. Friberg, K. Larsson (Eds.), Food Emulsions, 3rd ed., rev.expanded, Marcel Dekker, New York, 1997.
[11] R.G. Larson, Constitutive Equations For Polymer Melts and Solutions, Butterworths, Boston, 1988.
[12] R. Zenit, J.J. Feng, Hydrodynamic interactions among bubbles, drops, and particles in Non-Newtonian liquids, Annu. Rev. Fluid Mech. 50 (2018) 505–534, https://doi.org/10.1146/annurev-fluid-122316-045114.
[13] E.S.G. Shaqfeh, On the rheology of particle suspensions in viscoelastic fluids, AIChE J. 65 (2019) e16575, https://doi.org/10.1002/aic.16575.
[14] J.F. Morris, Toward a fluid mechanics of suspensions, Phys. Rev. Fluids 5 (2020) 110519, https://doi.org/10.1103/PhysRevFluids.5.110519.
[15] S. Dai, R.I. Tanner, Rheology of semi-dilute suspensions with a viscoelastic matrix, Rheol. Acta 59 (2020) 477–486, https://doi.org/10.1007/s00397-020-01217-5.
[16] M. Loewenberg, E.J. Hinch, Collision of two deformable drops in shear flow, J. Fluid Mech. 338 (1997) 299–315, https://doi.org/10.1017/S0022112097005016.
[17] F.R. Da Cunha, E.J. Hinch, Shear-induced dispersion in a dilute suspension of rough spheres, J. Fluid Mech. 309 (1996) 211–223, https://doi.org/10.1017/S0022112096001619.
[18] P.M. Kulkarni, J.F. Morris, Pair-sphere trajectories in finite-reynolds-number shear flow, J. Fluid Mech. 596 (2008) 413–435, https://doi.org/10.1017/S0022112007009627.
[19] H. Haddadi, J.F. Morris, Topology of pair-sphere trajectories in finite inertia suspension shear flow and its effects on microstructure and rheology, Phys. Fluids 27 (2015) 043302, https://doi.org/10.1063/1.4917030.
[20] F. Snijkers, R. Pasquino, J. Vermant, Hydrodynamic interactions between two equally sized spheres in viscoelastic fluids in shear flow, Langmuir 29 (2013) 5701–5713, https://doi.org/10.1021/la4006604.
[21] G.K. Batchelor, J.T. Green, The hydrodynamic interaction of two small freely-moving spheres in a linear flow field, J. Fluid Mech. 56 (1972) 375–400, https://doi.org/10.1017/S0022112072002927.
[22] C.L. Darabaner, S.G. Mason, Particle motions in sheared suspensions XXII: interactions of rigid spheres (experimental), Rheol. Acta 6 (1967) 273–284, https://doi.org/10.1007/BF01976445.
[23] A.R. Malipeddi, K. Sarkar, Shear-induced collective diffusivity down a concentration gradient in a viscous emulsion of drops, J. Fluid Mech. 868 (2019) 5–25, https://doi.org/10.1017/jfm.2019.122.
[24] A.R. Malipeddi, K. Sarkar, Shear-induced gradient diffusivity of a red blood cell suspension: effects of cell dynamics from tumbling to tank-treading, Soft Matter 17 (2021) 8523–8535, https://doi.org/10.1039/D1SM00938A.
[25] A.R. Malipeddi, K. Sarkar, Collective diffusivity in a sheared viscous emulsion: effects of viscosity ratio, Phys. Rev. Fluids 4 (2019) 093603, https://doi.org/10.1103/PhysRevFluids.4.093603.
[26] M. Zurita-Gotor, J. Bławzdziewicz, E. Wajnryb, Swapping trajectories: a new wall-induced cross-streamline particle migration mechanism in a dilute suspension of spheres, J. Fluid Mech. 592 (2007) 447–469, https://doi.org/10.1017/S0022112007008701.
[27] K. Sarkar, R.K. Singh, Spatial ordering due to hydrodynamic interactions between a pair of colliding drops in a confined shear, Phys. Fluids 25 (2013) 051702, https://doi.org/10.1063/1.4805082.
[28] P.M. Kulkarni, J.F. Morris, Suspension properties at finite Reynolds number from simulated shear flow, Phys. Fluids 20 (2008) 040602, https://doi.org/10.1063/1.2911017.
[29] P.O. Olapade, R.K. Singh, K. Sarkar, Pairwise interactions between deformable drops in free shear at finite inertia, Phys. Fluids 21 (2009) 063302, https://doi.org/10.1063/1.3153905.
[30] R.K. Singh, K. Sarkar, Effects of viscosity ratio and three dimensional positioning on hydrodynamic interactions between two viscous drops in a shear flow at finite inertia, Phys. Fluids 21 (2009) 103303, https://doi.org/10.1063/1.3253351.
[31] Y. Chen, C. Wang, Hydrodynamic interaction of two deformable drops in confined shear flow, Phys. Rev. E 90 (2014) 033010, https://doi.org/10.1103/PhysRevE.90.033010.
[32] G. D'Avino, P.L. Maffettone, Particle dynamics in viscoelastic liquids, J. Nonnewt. Fluid Mech. 215 (2015) 80–104, https://doi.org/10.1016/j.jnnfm.2014.09.014.
[33] S.-H. Chiu, T.-W. Pan, R. Glowinski, A 3D DLM/FD method for simulating the motion of spheres in a bounded shear flow of Oldroyd-B fluids, Comput. Fluids 172 (2018) 661–673, https://doi.org/10.1016/j.compfluid.2018.02.006.
[34] W.R. Hwang, M.A. Hulsen, H.E.H. Meijer, Direct simulations of particle suspensions in a viscoelastic fluid in sliding bi-periodic frames, J. Nonnewt. Fluid Mech. 121 (2004) 15–33, https://doi.org/10.1016/j.jnnfm.2004.03.008.
[35] Y.J. Choi, M.A. Hulsen, H.E.H. Meijer, An extended finite element method for the simulation of particulate viscoelastic flows, J. Nonnewt. Fluid Mech. 165 (2010) 607–624, https://doi.org/10.1016/j.jnnfm.2010.02.021.
[36] S. Yoon, M.A. Walkley, O.G. Harlen, Two particle interactions in a confined viscoelastic fluid under shear, J. Nonnewt. Fluid Mech. 185–186 (2012) 39–48, https://doi.org/10.1016/j.jnnfm.2012.07.003.
[37] H. Fahs, G. Ovarlez, X. Chateau, Pair-particle trajectories in a shear flow of a Bingham fluid, J. Nonnewt. Fluid Mech. 261 (2018) 171–187, https://doi.org/10.1016/j.jnnfm.2018.07.010.
[38] M. Firouznia, B. Metzger, G. Ovarlez, S. Hormozi, The interaction of two spherical particles in simple-shear flows of yield stress fluids, J. Nonnewt. Fluid Mech. 255 (2018) 19–38, https://doi.org/10.1016/j.jnnfm.2018.03.006.
[39] N. Aggarwal, K. Sarkar, Effects of matrix viscoelasticity on viscous and viscoelastic drop deformation in a shear flow, J. Fluid Mech. 601 (2008) 63–84, https://doi.org/10.1017/S0022112008000451.
[40] S. Guido, Shear-induced droplet deformation: effects of confined geometry and viscoelasticity, Curr. Opin. Colloid Interface Sci 16 (2011) 61–70, https://doi.org/10.1016/j.cocis.2010.12.001.
[41] A. Tarafder, A.R. Malipeddi, K. Sarkar, Pair interactions between viscous drops in a viscoelastic matrix in free shear: transition from passing to tumbling trajectories, J. Rheol. (N N Y) 66 (2022) 571–584, https://doi.org/10.1122/8.0000374.
[42] N. Paxton, W. Smolan, T. Böck, F. Melchels, J. Groll, T. Jungst, Proposal to assess printability of bioinks for extrusion-based bioprinting and evaluation of rheological properties governing bioprintability, Biofabrication 9 (2017) 044107, https://doi.org/10.1088/1758-5090/aa8dd8.
[43] S. Ramesh, O.L.A. Harrysson, P.K. Rao, A. Tamayol, D.R. Cormier, Y. Zhang, I. V. Rivero, Extrusion bioprinting: recent progress, challenges, and future opportunities, Bioprinting 21 (2021) e00116, https://doi.org/10.1016/j.bprint.2020.e00116.
[44] H. Li, C. Ruan, Y. Su, P. Jia, H. Wen, X. Zhu, Transient friction analysis of pressure waves propagating in power-law Non-Newtonian fluids, Appl. Sci. 14 (2024) 6331, https://doi.org/10.3390/app14146331.
[45] A.M. AlSofi, T.C. LaForce, M.J. Blunt, Sweep impairment due to polymers shear thinning, 2009. https://doi.org/10.2118/120321-MS.

[46] P.Y. Huang, J. Feng, H.H. Hu, D.D. Joseph, Direct simulation of the motion of solid particles in Couette and Poiseuille flows of viscoelastic fluids, J. Fluid Mech. 343 (1997) 73–94, https://doi.org/10.1017/S0022112097005764.
[47] M. Ravisankar, A.G. Correa, Y. Su, R. Zenit, Hydrodynamic interaction of a bubble pair in viscoelastic shear-thinning fluids, J. Nonnewt. Fluid Mech. 309 (2022) 104912, https://doi.org/10.1016/j.jnnfm.2022.104912.
[48] S. Hazra, A. Nath, S.K. Mitra, A.K. Sen, Dynamics of rigid particles in a confined flow of viscoelastic and strongly shear-thinning fluid at very small reynolds numbers, Phys. Fluids 33 (2021) 052001, https://doi.org/10.1063/5.0046729.
[49] S.M. Masiri, M. Bayareh, A.A. Nadooshan, Pairwise interaction of drops in shear-thinning inelastic fluids, Korea-Aust. Rheol. J. 31 (2019) 25–34, https://doi.org/10.1007/s13367-019-0003-8.
[50] N. Aggarwal, K. Sarkar, Deformation and breakup of a viscoelastic drop in a Newtonian matrix under steady shear, J. Fluid Mech. 584 (2007) 1–21, https://doi.org/10.1017/S0022112007006210.
[51] M.D. Chilcott, J.M. Rallison, Creeping flow of dilute polymer solutions past cylinders and spheres, J. Nonnewt. Fluid Mech. 29 (1988) 381–432, https://doi.org/10.1016/0377-0257(88)85062-6.
[52] S. Mukherjee, K. Sarkar, Lateral migration of a viscoelastic drop in a Newtonian fluid in a shear flow near a wall, Phys. Fluids 26 (2014) 103102, https://doi.org/10.1063/1.4897921.
[53] S. Mukherjee, K. Sarkar, Effects of matrix viscoelasticity on the lateral migration of a deformable drop in a wall-bounded shear, J. Fluid Mech. 727 (2013) 318–345, https://doi.org/10.1017/jfm.2013.251.
[54] K. Sarkar, W.R. Schowalter, Deformation of a two-dimensional viscoelastic drop at non-zero reynolds number in time-periodic extensional flows, J. Nonnewt. Fluid Mech. 95 (2000) 315–342, https://doi.org/10.1016/S0377-0257(00)00156-7.
[55] S.O. Unverdi, G. Tryggvason, A front-tracking method for viscous, incompressible, multi-fluid flows, J. Comput. Phys. 100 (1992) 25–37, https://doi.org/10.1016/0021-9991(92)90307-K.
[56] K. Sarkar, W.R. Schowalter, Deformation of a two-dimensional drop at non-zero Reynolds number in time-periodic extensional flows: numerical simulation, J. Fluid Mech. 436 (2001) 177–206, https://doi.org/10.1017/S0022112001004025.
[57] P. Szabo, J.M. Rallison, E.J. Hinch, Start-up of flow of a FENE-fluid through a 4:1:4 constriction in a tube, J. Nonnewt. Fluid Mech. 72 (1997) 73–86, https://doi.org/10.1016/S0377-0257(97)00023-2.
[58] S. Ramaswamy, L.G. Leal, The deformation of a viscoelastic drop subjected to steady uniaxial extensional flow of a Newtonian fluid, J. Nonnewt. Fluid Mech. 85 (1999) 127–163, https://doi.org/10.1016/S0377-0257(98)00212-2.
[59] H.-S. Dou, N. Phan-Thien, Negative wake in the uniform flow past a cylinder, Rheol. Acta 42 (2003) 383–409, https://doi.org/10.1007/s00397-003-0293-z.
[60] J.M. Kim, C. Kim, C. Chung, K.H. Ahn, S.J. Lee, Negative wake generation of FENE-CR fluids in uniform and Poiseuille flows past a cylinder, Rheol. Acta 44 (2005) 600–613, https://doi.org/10.1007/s00397-005-0442-7.
[61] D. Alghalibi, I. Lashgari, L. Brandt, S. Hormozi, Interface-resolved simulations of particle suspensions in newtonian, shear thinning and shear thickening carrier fluids, J. Fluid Mech. 852 (2018) 329–357, https://doi.org/10.1017/jfm.2018.532.
[62] X. Zhang, H. Liu, Y. Zhang, L. Wang, Direct numerical simulation of the sedimentation of a particle pair in a shear-thinning fluid, Phys. Rev. Fluids 5 (2020) 014304, https://doi.org/10.1103/PhysRevFluids.5.014304.
[63] N. Wang, H. Liu, C. Zhang, Deformation and breakup of a confined droplet in shear flows with power-law rheology, J. Rheol. (N N Y) 61 (2017) 741–758, https://doi.org/10.1122/1.4984757.
[64] S. Dhinakaran, M.S.N. Oliveira, F.T. Pinho, M.A. Alves, Steady flow of power-law fluids in a 1:3 planar sudden expansion, J. Nonnewt. Fluid Mech. 198 (2013) 48–58, https://doi.org/10.1016/j.jnnfm.2013.01.006.
[65] A. Lavrov, Flow of truncated power-law fluid between parallel walls for hydraulic fracturing applications, J. Nonnewt. Fluid Mech. 223 (2015) 141–146, https://doi.org/10.1016/j.jnnfm.2015.06.005.
[66] J.L. White, A.B. Metzner, Development of constitutive equations for polymeric melts and solutions, J. Appl. Polym. Sci. 7 (1963) 1867–1889, https://doi.org/10.1002/app.1963.070070524.
[67] R.K. Singh, K. Sarkar, Hydrodynamic interactions between pairs of capsules and drops in a simple shear: effects of viscosity ratio and heterogeneous collision, Phys. Rev. E 92 (2015) 063029, https://doi.org/10.1103/PhysRevE.92.063029.
[68] S. Guido, M. Simeone, Binary collision of drops in simple shear flow by computer-assisted video optical microscopy, J. Fluid Mech. 357 (1998) 1–20, https://doi.org/10.1017/S0022112097007921.
[69] E. Lac, A. Morel, D. Barthès-Biesel, Hydrodynamic interaction between two identical capsules in simple shear flow, J. Fluid Mech. 573 (2007) 149–169, https://doi.org/10.1017/S0022112006003739.
[70] E. Zana, L.G. Leal, The dynamics and dissolution of gas bubbles in a viscoelastic fluid, Int. J. Multiph. Flow 4 (1978) 237–262, https://doi.org/10.1016/0301-9322(78)90001-0.
[71] M. Marchioro, A. Acrivos, Shear-induced particle diffusivities from numerical simulations, J. Fluid Mech. 443 (2001) 101–128, https://doi.org/10.1017/S0022112001005122.
[72] A.M. Leshansky, J.F. Morris, J.F. Brady, Collective diffusion in sheared colloidal suspensions, J. Fluid Mech. 597 (2008) 305–341, https://doi.org/10.1017/S0022112007009834.
[73] H.A. Stone, Dynamics of drop deformation and breakup in viscous fluids, Annu. Rev. Fluid Mech. 26 (1994) 65–102, https://doi.org/10.1146/annurev.fl.26.010194.000433.
[74] E. Lac, D. Barthès-Biesel, Pairwise interaction of capsules in simple shear flow: three-dimensional effects, Phys. Fluids 20 (2008) 040801, https://doi.org/10.1063/1.2911695.
[75] C.J. Guido, E.S.G. Shaqfeh, The rheology of soft bodies suspended in the simple shear flow of a viscoelastic fluid, J. Nonnewt. Fluid Mech. 273 (2019) 104183, https://doi.org/10.1016/j.jnnfm.2019.104183.